PHYSICAL REVIEW APPLIED **11,** 044070 (2019)

Spin-Orbit-Torque Switching Mediated by an Antiferromagnetic Insulator

Hailong Wang,[†] Joseph Finley, Pengxiang Zhang, Jiahao Han, Justin T. Hou, and Luqiao Liu[*]
Department of Electrical Engineering and Computer Science, Massachusetts Institute of Technology, Cambridge, Massachusetts 02139, USA

(Received 21 November 2018; revised manuscript received 27 March 2019; published 22 April 2019)

We report the observation of antiferromagnetic insulator-mediated spin-orbit-torque switching in Pt/NiO/$Co_{1-x}Tb_x$ heterostructures. By measuring the current-induced shift in the magnetic hysteresis loops and the second-harmonic anomalous Hall resistance, we quantitatively determine the spin-orbit-torque efficiency in Pt/NiO/$Co_{1-x}Tb_x$ samples with different NiO thicknesses, uncovering a systematic evolution of the magnetic switching behavior. The measured spin-orbit-torque efficiency is enhanced in the low NiO thickness regime (1–2 nm), highlighting the efficient spin manipulation across a disordered antiferromagnetic insulator.

DOI: 10.1103/PhysRevApplied.11.044070

I. INTRODUCTION

Spin transport and magnetic dynamics in antiferromagnetic (AF) insulators have recently attracted wide research interest [1–7]. Contrary to the popular belief that AF materials are inactive elements for spin transport, recent experiments based on spin pumping [8,9], spin-torque ferromagnetic resonance [10], nonlocal spin transport [11,12], and the spin Seebeck effect [13–15] suggest efficient spin-current transmission can be realized in various AF systems via the mediation of AF exchange interactions. The large spin conductivity and the absence of charge conduction channels make AF insulators highly attractive for low-power spintronic applications. In particular, by using AF insulators as an insertion barrier in magnetic devices based on spin-orbit torque (SOT), one can potentially eliminate the shunting currents inside the free layer and minimize Joule heating [16]. In this work, we show initial experimental evidence toward this direction. Specifically, we utilize the current-induced SOT [17–19] in a Pt layer to switch a $Co_{1-x}Tb_x$ free layer across a thin AF insulator NiO. In the ultrathin spacer thickness regime (1–2 nm), we even observe an enhancement of the SOT efficiency compared with a Pt/$Co_{1-x}Tb_x$ bilayer. The realization of magnetic switching in Pt/NiO/$Co_{1-x}Tb_x$ heterostructures provides proof of AF insulator-mediated SOT, enabling promising material platforms and device structures for energy favorable spin manipulation.

II. CHARACTERIZATION OF MAGNETIC PROPERTIES

Current-induced SOT has been proven to be an efficient mechanism for magnetic moment reorientation [17–21]. In typical device structures, a clean, transparent interface between the SOT material and the magnetic electrode is critical to ensure a high transmission rate for spins. To verify whether the presence of an AF insulator barrier allows for the transmission of spin torque, we deposit Pt(5 nm)/NiO(0.5–10 nm)/$Co_{1-x}Tb_x$(4–10 nm)/SiN_x(5 nm) multilayers on oxidized Si substrates using magnetron sputtering. The different $Co_{1-x}Tb_x$ film thicknesses are chosen for optimal perpendicular magnetic anisotropy (PMA). The schematic of the film stacks is shown in Fig. 1(a), where the Pt layer acts as a spin current source and SiN_x is used as an insulating capping layer to avoid oxidation of the magnetic film. $Co_{1-x}Tb_x$ is chosen as the magnetic free layer because it can be deposited on a variety of underlayers and substrates while maintaining a robust PMA [22–28]. In our experiment, $Co_{1-x}Tb_x$ (CoTb in short for the rest of the work) with different chemical compositions is tested. We conclude that a Tb atomic ratio of $x = 0.23$ is optimal for achieving a square magnetic hysteresis loop. Figure 1(b) shows the results from vibrating-sample magnetometry (VSM) measurements, from which an effective out-of-plane anisotropy field $H_K \sim 6000$ Oe is determined. The devices are patterned into micrometer-size Hall bar structures by standard photolithography and lift-off processes [Fig. 1(c)] with a channel width of 10 μm. The anomalous Hall resistance R_H of a fabricated device as a function of applied out-of-plane magnetic field H_z is plotted in Fig. 1(d). The measured anomalous Hall resistance R_H is 0.3 Ω, while the coercivity is approximately 600 Oe, in agreement with the

---

[*] luqiao@mit.edu

[†] Current address: Center for Memory and Recording Research, University of California, San Diego, La Jolla, CA 92093, USA

VSM results. All of the measurements reported here are performed at room temperature.

III. SPIN-ORBIT-TORQUE-INDUCED MAGNETIC SWITCHING

As shown in Fig. 1(a), when an electrical charge current J_c flows through the Pt layer along the x direction, a spin current will be generated along the z axis with spin polarization $\boldsymbol{\sigma}$ oriented along the y axis by spin Hall effect, which will transport across the insulating NiO layer [29,30]. To check whether the spin current absorbed by the CoTb free layer J_s exerts any influence on its magnetic moment, we carry out current-induced magnetic switching measurements on a series of Hall bar devices. Results from Pt/NiO(t_{NiO})/CoTb/SiN$_x$ samples with the NiO thickness t_{NiO} varying between 0 and 5 nm are shown in Figs. 2(a)–2(e). In these measurements, an external dc magnetic field of $H_x = \pm 200$ Oe is applied along the current direction to give a deterministic switching polarity [17,31]. We apply millisecond current pulses J_{pulse} to minimize Joule heating. The anomalous Hall resistance is measured with a lower sensing current (approximately 0.5 mA) after each applied pulse. As expected, in the absence of the NiO layer [Fig. 2(a)], the CoTb magnetization reversibly switches between the $+z$ and $-z$ directions under positive and negative applied currents. The switching curves change polarity when the external dc magnetic field H_x is reversed, consistent with the mechanism of SOT-induced magnetic switching. With the insertion of a thin NiO layer between the Pt and CoTb layers, SOT-induced magnetic switching features still remain when the NiO thickness is smaller than 5 nm [Figs. 2(b)–2(d)]. In particular, for the samples with 0.5- and 1-nm thick NiO spacers, the magnitude of the switching current is similar to that of the Pt/CoTb sample, indicating a high transmission of the spin current. Meanwhile, for the NiO spacer thickness equal to or larger than 5 nm, no magnetic switching behavior is observed [Fig. 2(e)]. By comparing the R_H change in the current-induced switching experiment with that from the field switching experiments of Fig. 1(d), we determine that

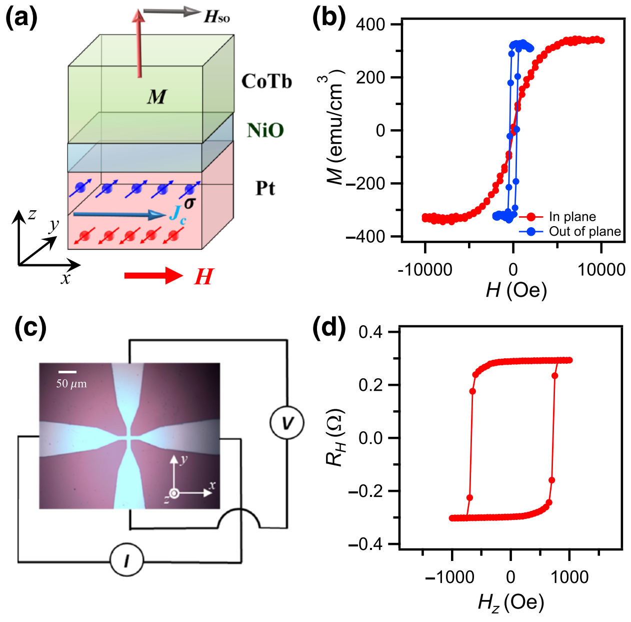

FIG. 1. (a) Schematic of SOT in Pt/NiO/CoTb heterostructures. The generated effective field H_{SO} is proportional to $\boldsymbol{\sigma} \times \boldsymbol{m}$. (b) Room temperature in-plane and out-of-plane magnetic hysteresis loops of Pt(5 nm)/NiO(1 nm)/CoTb(5 nm) sample measured by vibrating sample magnetometry. (c) Image of a patterned Pt(5 nm)/NiO(1 nm)/CoTb(5 nm)/SiN$_x$(3 nm) Hall bar device with an illustration of the SOT-induced magnetic switching measurement set up. The current is applied along the x axis and the anomalous Hall voltage is detected in the y direction. (d) The measured anomalous Hall resistance of Pt(5 nm)/NiO(1 nm)/CoTb(5 nm) Hall bar device as a function of out-of-plane magnetic field H_z.

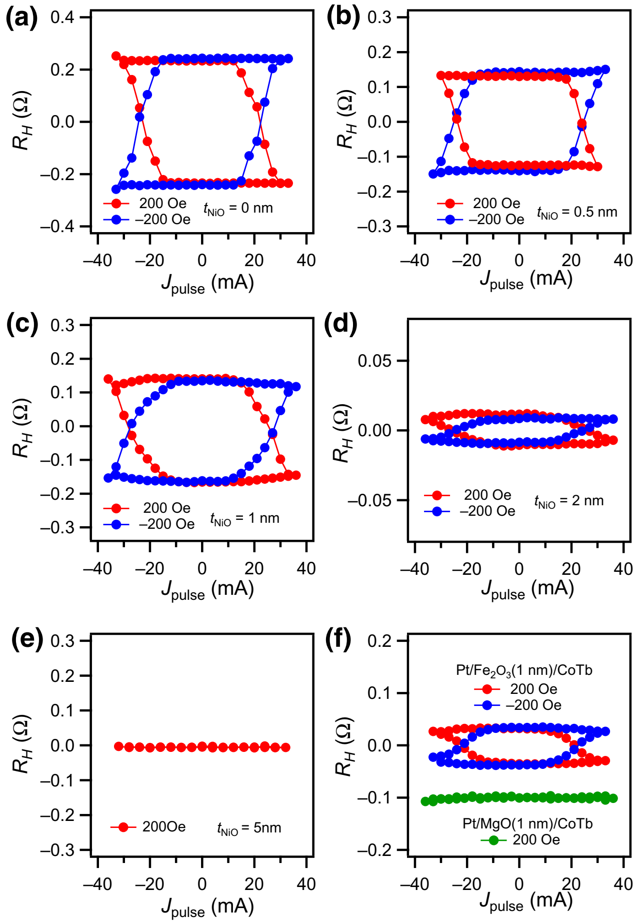

FIG. 2. (a)–(e) Separate SOT-induced magnetic switching curves under ±200 Oe in-plane bias field H_x of Pt/NiO(t_{NiO})/CoTb samples for $t_{\mathrm{NiO}} = 0$, 0.5, 1, 2, and 5 nm. (f) Control measurements of Pt/Fe$_2$O$_3$(1 nm)/CoTb and Pt/MgO(1 nm)/CoTb samples. The data for the Pt/MgO(1 nm)/CoTb sample is shifted vertically for clarity.

the portion of flipped magnetic domains during switching is 80%–50% in Figs. 2(a)–2(c) and 5% in Fig. 2(d). The decrease in the switching ratio of the 2-nm sample and the disappearance of magnetic switching in the 5-nm sample can be explained by spin memory loss [32] in the NiO layer due to defects and/or inhomogeneities in the thin film heterostructures.

In addition to NiO, it was recently reported that Fe_2O_3 also possesses AF ordering and supports spin current transport [12]. Therefore, we also perform the SOT-induced switching measurements in Pt/Fe_2O_3(1 nm)/CoTb heterostructures as shown in Fig. 2(f). Clear magnetic switching features can be observed. To confirm that the observed magnetic switchings in Pt/NiO/CoTb and Pt/Fe_2O_3/CoTb samples are related to the AF ordering of the employed insulators, we perform a control experiment by inserting a 1-nm diamagnetic MgO layer between Pt and CoTb. As shown in Fig. 2(f), no magnetic switching is observed in the control sample, which is in sharp contrast with results obtained in the AF-insulator-based heterostructures. This unambiguously demonstrates the significant role played by the AF insulator in achieving efficient magnetic control in these samples.

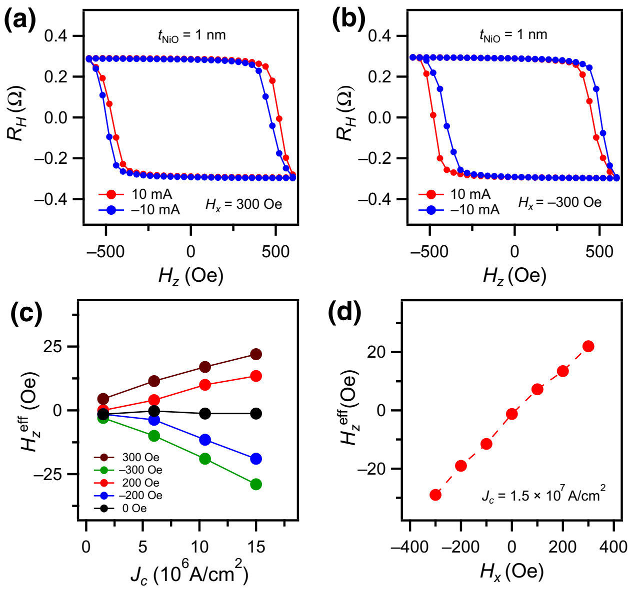

FIG. 3. Current-induced shift of anomalous Hall resistance loops of Pt/NiO(1 nm)/CoTb sample under bias fields (a) $H_x = 300$ Oe and (b) $H_x = -300$ Oe. The applied dc currents are ±10 mA. (c) The measured H_z^{eff} in the Pt/NiO(1 nm)/CoTb sample as a function of current density J_c under different bias fields $H_x = 0$, ± 200, and ± 300 Oe. (d) The measured H_z^{eff} as a function of the applied in-plane bias field H_x at $J_c = 1.5 \times 10^7$ A/cm^2.

IV. QUANTITATIVE DETERMINATION OF SPIN-ORBIT-TORQUE EFFICIENCY

The threshold current of multidomain samples is influenced by extrinsic factors such as the domain-wall depinning field and the applied in-plane field. Therefore, in general, it is difficult to precisely determine the SOT efficiency from the magnitude of the switching current. To quantitatively measure SOT efficiencies in the series of Pt/NiO(t_{NiO})/CoTb samples, we utilize two independent experimental techniques: measurement on the current-induced hysteresis loop shift of the $R_H - H_z$ curve and second-harmonic measurement of the anomalous Hall resistance. In the first approach, we apply an in-plane bias field H_x along the current direction and measure the horizontal shift of the $R_H - H_z$ loops induced by the damping-like term of the effective SOT field H_z^{eff} [33]. Figures 3(a) and 3(b) show the field-induced magnetic switching curves for the Pt(5 nm)/NiO(1 nm)/CoTb(5 nm) sample under $H_x = \pm 300$ Oe, respectively. It is noted that the center of the $R_H - H_z$ curve shifts to the positive (negative) direction in the presence of a positive (negative) 10-mA current. When the in-plane field reverses, the shift of the magnetic hysteresis loop changes direction, which is consistent with the expected magnetic domain-wall chirality change under a magnetic field. We further measure the $R_H - H_z$ hysteresis loops under a series of applied currents with $H_x = 0$, ±200 and ±300 Oe. As shown in Fig. 3(c), for each different in-plane field, H_z^{eff} scales linearly with the applied current. The dependence of H_z^{eff} on H_x for a fixed applied current density of $J_c = 1.5 \times 10^7$ A/cm^2 is summarized in Fig. 3(d). The increase of H_z^{eff} with the applied in-plane field is related to the Dzyaloshinskii-Moriya interaction (DMI) at the interface between the magnetic layer (CoTb) and the neighboring layers, which can create stable Néel-type domain walls with a certain type of chirality [22,34]. For $H_x = 0$, domain walls do not have a preference for magnetic switching, leading to zero effective field H_z^{eff}. As H_x increases and starts to overcome the effective DMI field, domain walls start to move in the direction that favors magnetic switching [20,21,34–36]. Due to the limit on the maximum H_x that can be reached by our vector field electromagnet system, we did not observe the expected saturation of H_z^{eff}. Here, we use the measured H_z^{eff} under the maximum bias field $H_x = \pm 300$ Oe to provide a lower bound estimation on the SOT efficiency characterized by J_s/J_c, which can be calculated with material parameters using the formula [33,37]

$$\frac{J_s}{J_c} = \frac{2}{\pi} \frac{2e\mu_0 M_s H_z^{eff} t_{CoTb}}{J_c \hbar} \tag{1}$$

where e is the electron charge, μ_0 is the vacuum permeability, M_S is the saturated magnetization, t_{CoTb} is the thickness of the CoTb layer, J_c is the electrical current density flowing through the Pt layer after considering the electrical shunting effect of CoTb, and $\hbar$ is the reduced Planck's constant. For $t_{NiO} = 1$ and 2 nm, the obtained

J_s/J_c in Pt/NiO(t_{NiO})/CoTb samples are determined to be 0.051 ± 0.005 and 0.034 ± 0.003, respectively, which are larger than the $J_s/J_c = 0.017 \pm 0.002$ measured in the Pt/CoTb bilayer structure without a NiO insertion.

The second experimental approach that we employ to calibrate the effective field is the second-harmonic measurement of the anomalous Hall resistance [38–42]. When applying an alternating current (ac) through the device, an alternating field H_z^{eff} proportional to $\boldsymbol{\sigma} \times \boldsymbol{m}$ generated from the spin Hall effect in the Pt film can cause the CoTb magnetization $\boldsymbol{m}$ to oscillate around the equilibrium position, giving rise to a second-harmonic anomalous Hall resistance $R_{2\omega}$. Because only one external magnetic field is required for this experiment, we can apply a larger field H_x along the current direction to overcome the magnetic anisotropy field H_K. In the regime where $|H_x| > H_K$, the observed second-harmonic anomalous Hall resistance can be simplified to the following formula [40,41]

$$R_{2\omega} = \frac{1}{2}\frac{R_H H_z^{\mathrm{eff}}}{(|H_x| - H_K)}. \tag{2}$$

The amplitude of the ac current is 5 mA with a frequency of $f = 160$ Hz. Figure 4(a) shows the measured $R_{2\omega}$ as a function of the external in-plane field H_x for the Pt/NiO(1 nm)/CoTb sample. In the large in-plane field regime ($|H_x| > H_K$), the measured $R_{2\omega}$ scales well with $1/(|H_x| - H_K)$ for $t_{\mathrm{NiO}} = 0.5$, 1, and 2 nm as shown by the gray fitting curves in Fig. 4(b). Here, we can exclude the small contributions from the planar Hall effect and the anomalous Nernst effect via the exhibited field and in-plane angular dependence of the measured $R_{2\omega}$ [43]. Utilizing the fitted H_z^{eff} and Eq. (1), we can determine the SOT efficiency J_s/J_c to be 0.088 ± 0.009 and 0.076 ± 0.008 for $t_{\mathrm{NiO}} = 1$ and 2 nm, respectively, which is higher than the value of the Pt/CoTb bilayer structure.

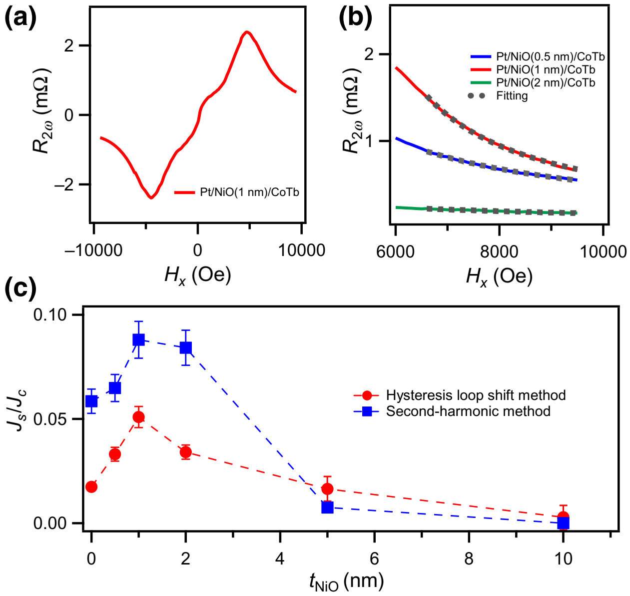

FIG. 4. (a) In-plane field dependence of the measured second-harmonic resistance of the Pt/NiO(1 nm)/CoTb sample. The amplitude of the input ac current is 5 mA with a frequency $f = 160$ Hz. (b) The measured second-harmonic resistances of Pt/NiO(t_{NiO})/CoTb samples with $t_{\mathrm{NiO}} = 0.5$, 1, and 2 nm in the high-field regime where $H_x \geq 6000$ Oe. The gray dash lines represent fitting curves proportional to $1/(|H_x| - H_K)$ when CoTb films are in a single domain state. (c) NiO spacer thickness dependence of the charge-to-spin conversion efficiency J_s/J_c measured by the shift of magnetic hysteresis loops and second-harmonic resistance analysis methods in Pt/NiO/CoTb devices.

The evolution of J_s/J_c with NiO spacer thickness t_{NiO} measured by both experimental approaches is summarized in Fig. 4(c). As mentioned above, J_s/J_c measured by the shift of the magnetic hysteresis loop is limited by the unsaturated H_z^{eff} under a small in-plane bias field, which represents a lower bound estimation for the real charge-to-spin conversion efficiency. Despite this, J_s/J_c values from the two experimental approaches show very similar trends: they first increase and reach a maximum when $t_{\mathrm{NiO}} = 1$ nm. As the NiO thickness increases further, J_s/J_c starts to decay and finally becomes negligibly small. The increase of spin-torque efficiency with an ultrathin NiO insertion layer can be explained by an improved spin mixing conductance at the Pt/NiO and NiO/CoTb interfaces, compared with a direct Pt/CoTb contact. It is worth noting that our prepared NiO ultrathin samples with thicknesses t_{NiO} of 1–2 nm are disordered. They exhibit geometrical frustration instead of a long-range AF ordering with a preferred magnetic orientation, therefore, leading to a rapid relaxation of the injected spin currents as well as a short spin decay length compared with some previous studies [10,44–46]. While the short range magnetic fluctuation inside ultrathin NiO films allows for transparent transmission of magnon spin current, AF ordering gets restored with thicker NiO insertions ($t_{\mathrm{NiO}} \geq 5$ nm) and the large magnon band gap prohibits the transmission of low-energy spin current [47]. Although the observed enhancement in spin transmission efficiency in the low NiO thickness regime was also previously reported in inverse spin Hall effect studies [8,14,15], the robust magnetic switching features we show here unambiguously demonstrate the technical significance of spin-torque transfer in AF insulators and pave the way toward future energy favorable spintronic devices.

V. CONCLUSION

In conclusion, we report the observation of AF insulator-mediated spin-orbit-torque magnetic switching in a series of Pt/NiO/CoTb samples, demonstrating the optimal interfacial conditions and a large spin transport efficiency. By measuring the current-induced shift of the magnetic hysteresis loops and the second-harmonic anomalous Hall resistance, we determine the spin-torque efficiency and observe an enhancement in the charge-to-spin conversion ratio with the insertion of an ultrathin NiO layer. Our results highlight the significant role played by an AF insulator in achieving energy favorable magnetic control and suggest an alternative path toward next generation magnetic switching devices.

ACKNOWLEDGEMENT

We acknowledge support from National Science Foundation under Grant No. ECCS-1808826 and WESTERN DIGITAL TECHNOLOGIES, INC. The material synthesis and characterization were partially supported by the National Science Foundation under Grant No. DMR 14-19807 through the MRSEC shared facilities.

[1] P. Wadley, *et al.*, Electrical switching of an antiferromagnet, Science **351**, 587 (2016).

[2] T. Jungwirth, X. Marti, P. Wadley, and J. Wunderlich, Antiferromagnetic spintronics, Nat. Nanotechnol. **11**, 231 (2016).

[3] V. Baltz, A. Manchon, M. Tsoi, T. Moriyama, T. Ono, and Y. Tserkovnyak, Antiferromagnetic spintronics, Rev. Mod. Phys. **90**, 015005 (2018).

[4] J. Železný, P. Wadley, K. Olejník, A. Hoffmann, and H. Ohno, Spin transport and spin torque in antiferromagnetic devices, Nat. Phys. **14**, 220 (2018).

[5] L. Šmejkal, Y. Mokrousov, B. Yan, and A. H. MacDonald, Topological antiferromagnetic spintronics, Nat. Phys. **14**, 242 (2018).

[6] R. Cheng, J. Xiao, Q. Niu, and A. Brataas, Spin Pumping and Spin-Transfer Torques in Antiferromagnets, Phys. Rev. Lett. **113**, 057601 (2014).

[7] S. Takei, B. I. Halperin, A. Yacoby, and Y. Tserkovnyak, Superfluid spin transport through antiferromagnetic insulators, Phys. Rev. B **90**, 094408 (2014).

[8] H. L. Wang, C. H. Du, P. C. Hammel, and F. Y. Yang, Antiferromagnonic Spin Transport from $Y_3Fe_5O_{12}$ Into NiO, Phys. Rev. Lett. **113**, 097202 (2014).

[9] C. Hahn, G. de Loubens, O. Klein, M. Viret, V. V. Naletov, and J. B. Youssef, Conduction of spin currents through insulating antiferromagnetic oxides, Europhys. Lett. **108**, 57005 (2014).

[10] T. Moriyama, S. Takei, M. Nagata, Y. Yoshimura, N. Matsuzaki, T. Terashima, Y. Tserkovnyak, and T. Ono, Antidamping spin transfer torque through epitaxial nickel oxide, Appl. Phys. Lett. **106**, 162406 (2015).

[11] W. Yuan, Q. Zhu, T. Su, Y. Yao, W. Xing, Y. Chen, Y. Ma, X. Lin, J. Shi, R. Shindou, X. C. Xie, and W. Han, Experimental signatures of spin superfluid ground state in canted antiferromagnet Cr_2O_3 via nonlocal spin transport, Sci. Adv. **4**, eaat1098 (2018).

[12] R. Lebrun, A. Ross, S. A. Bender, A. Qaiumzadeh, L. Baldrati, J. Cramer, A. Brataas, R. A. Duine, and M. Kläui, Tunable long-distance spin transport in a crystalline antiferromagnetic iron oxide, Nature **561**, 222 (2018).

[13] S. M. Wu, W. Zhang, A. KC, P. Borisov, J. E. Pearson, J. S. Jiang, D. Lederman, A. Hoffmann, and A. Bhattacharya, Antiferromagnetic Spin Seebeck Effect, Phys. Rev. Lett. **116**, 097204 (2016).

[14] W. Lin, K. Chen, S. Zhang, and C L Chien, Enhancement of Thermally Injected Spin Current Through an Antiferromagnetic Insulator, Phys. Rev. Lett. **116**, 186601 (2016).

[15] Z. Qiu, D. Hou, J. Barker, K. Yamamoto, O. Gomonay, and E. Saitoh, Spin colossal magnetoresistance in an antiferromagnetic insulator, Nat. Mater. **17**, 577 (2018).

[16] D. M. Bromberg, H. E. Sumbul, J.-G. Zhu, and L. Pileggi, All-magnetic magnetoresistive random access memory based on four terminal mCell device, J. Appl. Phys. **117**, 17B510 (2015).

[17] I. M. Miron, K. Garello, G. Gaudin, P.-J. Zermatten, M. V. Costache, S. Auffret, S. Bandiera, B. Rodmacq, A. Schuhl, and P. Gambardella, Perpendicular switching of a single ferromagnetic layer induced by in-plane current injection, Nature **476**, 189 (2011).

[18] L. Liu, C.-F. Pai, Y. Li, H. W. Tseng, D. C. Ralph, and R. A. Buhrman, Spin-torque switching with the giant spin Hall effect of tantalum, Science **336**, 555 (2012).

[19] S. Fukami, T. Anekawa, C. Zhang, and H. Ohno, A spin-orbit torque switching scheme with collinear magnetic easy axis and current configuration, Nat. Nanotechnol. **11**, 621 (2016).

[20] S. Emori, U. Bauer, S. M. Ahn, E. Martinez, and G. S. D. Beach, Current-driven dynamics of chiral ferromagnetic domain walls, Nat. Mater. **12**, 611 (2013).

[21] K. S. Ryu, L. Thomas, S. H. Yang, and S. Parkin, Chiral spin torque at magnetic domain walls, Nat. Nanotechnol. **8**, 527 (2013).

[22] J. Finley and L. Liu, Spin-Orbit-Torque Efficiency in Compensated Ferrimagnetic Cobalt-Terbium Alloys, Phys. Rev. Appl. **6**, 054001 (2016).

[23] K. Ueda, M. Mann, C.-F. Pai, A. J. Tan, and G. S. D. Beach, Spin-orbit torques in Ta/Tb_xCo_{100-x} ferrimagnetic alloy films with bulk perpendicular magnetic anisotropy, Appl. Phys. Lett. **109**, 232403 (2016).

[24] R. Mishra, J. Yu, X. Qiu, M. Motapothula, T. Venkatesan, and H. Yang, Anomalous Current-Induced Spin Torques in Ferrimagnets Near Compensation, Phys. Rev. Lett. **118**, 167201 (2017).

[25] N. Roschewsky, T. Matsumura, S. Cheema, F. Hellman, T. Kato, S. Iwata, and S. Salahuddin, Spin-orbit torques in ferrimagnetic GdFeCo alloys, Appl. Phys. Lett. **109**, 112403 (2016).

[26] K. Ueda, M. Mann, P. W. P. de Brouwer, D. Bono, and G. S. D. Beach, Temperature dependence of spin-orbit torques across the magnetic compensation point in a ferrimagnetic TbCo alloy film, Phys. Rev. B **96**, 064410 (2017).

[27] T. H. Pham, S.-G. Je, P. Vallobra, T. Fache, D. Lacour, G. Malinowski, M.-C. Cyrille, G. Gaudin, O. Boulle, M. Hehn, J.-C. Rojas-Sánchez, and S. Mangin, Thermal Contribution to the Spin-Orbit Torque in Metallic-Ferrimagnetic Systems, Phys. Rev. Appl. **9**, 064032 (2018).

[28] S.-G. Je, J.-C. Rojas-Sánchez, T. H. Pham, P. Vallobra, G. Malinowski, D. Lacour, T. Fache, M.-C. Cyrille, D.-Y. Kim, S.-B. Choe, M. Belmeguenai, M. Hehn, S. Mangin, G. Gaudin, and O. Boulle, Spin-orbit torque-induced

switching in ferrimagnetic alloys: Experiments and modeling, Appl. Phys. Lett. **112**, 062401 (2018).

[29] S.-L. Zhang and S. F. Zhang, Spin convertance at magnetic interfaces, Phys. Rev. B **86**, 214424 (2012).

[30] S. M. Rezende, R. L. Rodríguez-Suárez, and A. Azevedo, Diffusive magnonic spin transport in antiferromagnetic insulators, Phys. Rev. B **93**, 054412 (2016).

[31] L. Liu, O. J. Lee, T. J. Gudmundsen, D. C. Ralph, and R. A. Buhrman, Current-Induced Switching of Perpendicularly Magnetized Magnetic Layers Using Spin Torque from the Spin Hall Effect, Phys. Rev. Lett. **109**, 096602 (2012).

[32] J.-C. Rojas-Sánchez, N. Reyren, P. Laczkowski, W. Savero, J.-P. Attané, C. Deranlot, M. Jamet, J.-M. George, L. Vila, and H. Jaffrès, Spin Pumping and Inverse Spin Hall Effect in Platinum: The Essential Role of Spin-Memory Loss at Metallic Interface, Phys. Rev. Lett. **112**, 106602 (2014).

[33] C.-F. Pai, M. Mann, A. J. Tan, and G. S. D. Beach, Determination of spin torque efficiencies in heterostructures with perpendicular magnetic anisotropy, Phys. Rev. B **93**, 144409 (2016).

[34] T. Tono, T. Taniguchi, K.-J. Kim, T. Moriyama, A. Tsukamoto, and T. Ono, Chiral magnetic domain wall in ferrimagnetic GdFeCo wires, Appl. Phys. Express **8**, 073001 (2015).

[35] P. P. J. Haazen, E. Murè, J. H. Franken, R. Lavrijsen, H. J. M. Swagten, and B. Koopmans, Domain wall depinning governed by the spin Hall effect, Nat. Mater. **12**, 299 (2013).

[36] O. J. Lee, L. Liu, C. F. Pai, Y. Li, H. W. Tseng, P. G. Gowtham, J. P. Park, D. C. Ralph, and R. A. Buhrman, Central role of domain wall depinning for perpendicular magnetization switching driven by spin torque from the spin Hall effect, Phys. Rev. B **89**, 024418 (2014).

[37] A. Thiaville, S. Rohart, É Jué, V. Cros, and A. Fert, Dynamics of Dzyaloshinskii domain walls in ultrathin magnetic films, Europhys. Lett. **100**, 57002 (2012).

[38] K. Garello, I. M. Miron, C. O. Avci, F. Freimuth, Y. Mokrousov, S. Blügel, S. Auffret, O. Boulle, G. Gaudin, and P. Gambardella, Symmetry and magnitude of spin-orbit torques in ferromagnetic heterostructures, Nat. Nanotechnol. **8**, 587 (2013).

[39] J. Kim, J. Sinha, M. Hayashi, M. Yamanouchi, S. Fukami, T. Suzuki, S. Mitani, and H. Ohno, Layer thickness dependence of the current-induced effective field vector in Ta|CoFeB|MgO, Nat. Mater. **12**, 240 (2013).

[40] Y. Fan, P. Upadhyaya, X. Kou, M. Lang, S. Takei, Z. Wang, J. Tang, L. He, L. T. Chang, M. Montazeri, G. Yu, W. Jiang, T. Nie, R. N. Schwartz, Y. Tserkovnyak, K. L. Wang, Magnetization switching through giant spin-orbit torque in a magnetically doped topological insulator heterostructure, Nat. Mater. **13**, 699 (2014).

[41] T. Schulz, K. Lee, B. Krüger, R.-L. Conte, G. V. Karnad, K. Garcia, L. Vila, B. Ocker, D. Ravelosona, and M. Kläui, Effective field analysis using the full angular spin-orbit torque magnetometry dependence, Phys. Rev. B **95**, 224409 (2017).

[42] U. H. Pi, K. W. Kim, J. Y. Bae, S. C. Lee, Y. J. Cho, K. S. Kim, and S. Seo, Tilting of the spin orientation induced by Rashba effect in ferromagnetic metal layer, Appl. Phys. Lett. **97**, 162507 (2010).

[43] Q. Shao, G. Yu, Y.-W. Lan, Y. Shi, M.-Y. Li, C. Zheng, X. Zhu, L.-J. Li, P. K. Amiri, and K. L. Wang, Strong Rashba-Edelstein effect-induced spin-orbit torques in monolayer transition metal dichalcogenide/ferromagnet bilayers, Nano Lett. **16**, 7514 (2016).

[44] T. Moriyama, K. Oda, T. Ohkochi, M. Kimata, and T. Ono, Spin torque control of antiferromagnetic moments in NiO, Sci. Rep. **8**, 14167 (2018).

[45] T. Ikebuchi, T. Moriyama, H. Mizuno, K. Oda, and T. Ono, Spin current transmission in polycrystalline NiO films, Appl. Phys. Express **11**, 073003 (2018).

[46] Y.-M. Hung, C. Hahn, H. Chang, M. Z. Wu, H. Ohldag, and A. D. Kent, Spin transport in antiferromagnetic NiO and magnetoresistance in $Y_3Fe_5O_{12}$/NiO/Pt structures, AIP Adv. **7**, 055903 (2017).

[47] Z. Qiu, J. Li, D. Hou, E. Arenholz, A. T. N'Diaye, A. Tan, K. Uchida, K. Sato, S. Okamoto, Y. Tserkovnyak, Z. Q. Qiu, and E. Saitoh, Spin-current probe for phase transition in an insulator, Nat. Commun. **7**, 12670 (2016).